# From bare Ge nanowire to Ge/Si core/shell nanowires: A first-principles study

R. Peköz* and J.-Y. Raty
*Department of Physics, FNRS–University of Liège, Sart-Tilman 4000, Belgium*
(Received 13 July 2009; revised manuscript received 23 September 2009; published 14 October 2009)

Germanium/Germanium-Silicon core/shell nanowires are expected to play an important role in future electronic devices. We use first-principles plane-wave calculations within density-functional theory in the generalized gradient approximation to investigate the structural and electronic properties of bare and H-passivated Ge nanowires and core/shell Ge/Ge-Si, Ge/Si, and Si/Ge nanowires. The diameters of the nanowires considered are in the range of 0.6–2.9 nm and oriented along [110] and [111] directions. The diameter, the surface passivation, and the substitutional effects on the binding energy, band structure, and effective mass are extensively investigated considering the relative contribution of quantum confinement and surface effects.

DOI: 10.1103/PhysRevB.80.155432 PACS number(s): 61.46.Km, 73.22.−f, 71.30.+h

## I. INTRODUCTION

Nanowires (NWs) are among the most interesting nanostructures as the charge carriers are confined in two directions but are still free to move along the wire. Their very large aspect ratio results in many interesting properties that allow for different applications from their bulk or quantum dots forms. The range of potential applications of NWs keeps growing and includes developments in the fields of optoelectronics,[1,2] device miniaturization,[3] field-effect transistors,[4,5] and photovoltaic cells.[6–8]

Since Si and Ge have many common properties such as adopting the diamond crystal structure, having the same number of valence electrons or having indirect band gaps, they are used jointly in developing technologies and applications. In the literature, Ge and Si NWs grown along different directions with or without hydrogen saturation have been extensively studied both experimentally and theoretically.[9–16] However, the type of surface reconstruction and the quantum confinement effects on nanowires remain important topics as Si NWs with diameters down to 1 nm were recently synthesized,[17,18] emphasizing both the quantum confinement and the surface effects.

Recently, core/shell type nanowires have been drawing most of the interest of the NW community. Although many experimental studies have been conducted on the synthesis and characterization of core/shell heterostructured nanowires such as GaAs/AlGaAs, ZnO/$TiO_2$, ZnO/ZnS, GaN/GaP, theoretical investigations are not numerous.[19–25] After the experimental work of Lauhon *et al.*[26] on core/multishell nanowire structures, Ge-Si core/shell heterostructures have come through for their potential applications in nanowire-based devices. Only a few theoretical investigations of this system have been published so far. Musin and Wang[27] have computed the composition and size effects on the band-gap energy of Ge/Si and Si/Ge core/shell nanowires with orientations in the [110] and [111] directions, highlighting the nonlinear composition dependence of the band-gap energy against the NW's diameter and the shell thickness. Migas and Borisenko[28] have further discussed the direct vs indirect band-gap electronic structure of fully hydrogen-passivated SiGe, Ge/Si, and Si/Ge core/shell NWs in comparison with pure Si and Ge NWs oriented in the [001] direction.

In the present paper, we describe the structural, energetic, and electronic properties of Ge/Ge-Si core/shell NWs computed using first-principles calculations within the generalized gradient approximation (GGA). Our calculations include the surface reconstruction for bare Ge NWs, the effect of the hydrogen passivation of the surface, the relationship between the band gap and the diameter of the NWs, and the presence of substitutional Si atoms on the surface of the wire. We consider nanowires which have their axes oriented in both the [110] and the [111] directions[29] and with diameters ranging from 0.6 to 2.9 nm.[30]

## II. METHOD

We have performed first-principles calculations based on density-functional theory (DFT) (Ref. 31) using projector augmented wave potentials.[32] The exchange correlation was described in the[33] GGA using the PW91 (Ref. 34) functional as implemented in the VASP code.[35] A plane-wave expansion of the wave functions up to a kinetic-energy cutoff of 325 eV has been employed in order to reach a convergence of the total energy within less than $10^{-5}$ eV/atom. The nanowire geometries are initially constructed from the bulk diamond structure. With these settings, the bulk properties of germanium and silicon, such as their lattice constant and band structure are fully converged. As expected with the GGA approximation, the equilibrium lattice constants are overestimated. The calculated lattice parameter of bulk Ge is 5.77 Å which is 2% larger than the experimental value but very close to the other theoretical lattice constants.[36,37] In the present GGA-DFT calculation, the bulk Ge gap vanishes similarly to what was obtained in Ref. 38 and the indirect band gap of bulk Si is found to be equal to 0.63 eV. The width of the band gap is thus underestimated by about 0.66 eV in bulk Ge and 0.47 eV in Si. We performed test calculations with other functionals and found that the Wu-Cohen functional yields a finite, but still underestimated, energy gap of 0.34 eV for bulk Ge. The shape of the band structure is, however, similar to the results from a PW91 functional calculation. The Brillouin zone integration is performed using the Monkhorst-Pack scheme[39] with $(1\times1\times13)$ mesh points. The systems are constructed from diamond supercells. Due to the periodic boundary conditions, a ~10 Å vacuum space

 ©2009 The American Physical Society

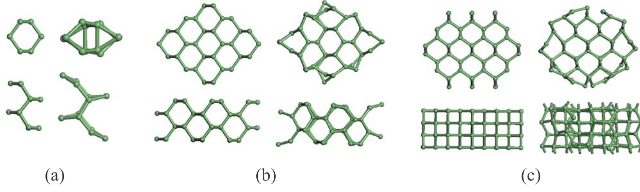


FIG. 1. (Color online) Bare Ge NWs oriented along [110] directions. Initial and optimized geometries are on the left and right for each type, respectively. Top and side views are on the upper and lower panels, respectively. (a) $Ge_{12}$, (b) $Ge_{60}$, and (c) $Ge_{76}$.

is used to prevent the spurious interactions between adjacent wire replicas. The geometry optimizations were performed using the conjugate-gradient method to minimize the total energy and the atomic forces, and were stopped when all residual forces were smaller than 0.001 eV/Å.

## III. RESULTS

The surface passivation of nanowires has significant effects on the physical and chemical properties of nanowires. The saturation of surface dangling bonds with hydrogen atoms, the growth directions and the diameters of the nanowires change the band-energy properties, and change the charge density which is important to understand the surface reactions. Generally, bare nanowires exhibit a metallic behavior because of the presence of dangling bonds on the surface, while hydrogen-passivated wires are semiconducting. These unsaturated surface bonds are known to form surface states with energies located in the band gap. Arantes and Fazzio[15] have studied the surface reconstruction of Ge NWs oriented in the [110] and have found that only the wire with the largest diameter (2.5 nm) had a band gap of 0.17 eV, the other wires being metallic. Durgun *et al.*[40] investigated both bare and hydrogen-terminated Si nanowires oriented along the [001] direction. Their calculations predicted that whereas bare Si NWs are metallic except for a very small diameter in which case it is semiconducting (band-gap energy of 0.6 eV), all hydrogen-passivated NWs were semiconducting.

In order to further understand the effect of surface reconstructions onto Ge NWs, we investigated both bare and hydrogen-passivated NWs with their axes oriented in the [110] and [111] directions (hereafter denoted by [110]-Ge and [111]-Ge). Figure 1 shows the initial and optimized geometries of some of the bare Ge NWs with different shapes that we considered.[41] It can be seen on this figure that the optimized NWs prefer to form dimers where possible, and instead of keeping steplike features on the surfaces, they tend to locally form $sp^2$ bonds to minimize the total energy. This can be understood by noticing that the dimers form in the case of two neighboring Ge atoms with two dangling bonds each, while the $sp^2$ like geometry appears at places where neighboring Ge atoms have only one dangling bond. Contrary to the wide belief that bare Ge NWs are metallic, unpassivated [110]-$Ge_{12}$ and [110]-$Ge_{32}$ have band gaps as large as 0.78 and 0.36 eV, respectively (see Table I). Whereas the smallest one ($Ge_{12}$) has an indirect band gap, the other has a band gap at the Z point (see Fig. 2). These results for

TABLE I. The cohesive energy per Ge atom ($E_c$ in eV) and minimum of the band-gap energy ($E_g$ in eV and M, I, and D are for metallic, indirect and direct, respectively) are tabulated for different Ge NWs.

| Wire axis | Ge NWs | $E_c$ (eV/atom) | $E_g$ (eV) |
|---|---|---|---|
| [110] | $Ge_{12}$ | 3.22 | 0.71 (I) |
| | $Ge_{32}$ | 3.35 | 0.36 (D) at Z point |
| | $Ge_{48}$ | 3.39 | M |
| | $Ge_{60}$ | 3.42 | M |
| | $Ge_{76}$ | 3.44 | M |
| | $Ge_{96}$ | 3.47 | M |
| | $Ge_{140}$ | 3.52 | M |
| [111] | $Ge_{74}$ | 3.39 | M |
| | $Ge_{138}$ | 3.49 | M |

[110]-$Ge_{12}$ and [110]-$Ge_{32}$ nanowires can be attributed to the extremely small diameters that produce strong deviations from the initial diamond structure. In Table I the cohesive energies per Ge atom of the nonpassivated Ge NWs are presented. They are calculated as

$$E_c = E[\mathrm{Ge_{NW}}]/n_{\mathrm{Ge}} - E[\mathrm{Ge}_{at}], \tag{1}$$

where $E[\mathrm{Ge}_{at}]$ is the energy of a single, isolated Ge atom, $E[\mathrm{Ge_{NW}}]$ is the total energy of the optimized Ge NWs and $n_{\mathrm{Ge}}$ is the total number of Ge atoms in the wire. It is obvious that negative cohesive energies mean that the wire structures are stable with respect to their free atoms. The calculated $E_c$ values decrease with the number of Ge atoms to converge toward the bulk value, as expected.[42]

The present results have additional information for small diameter unsaturated Ge NWs when compared with Ref. 15

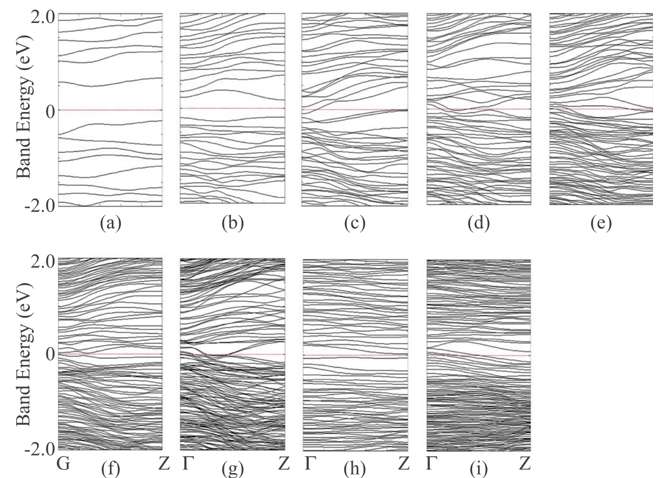


FIG. 2. (Color online) Energy band structures of nonpassivated Ge NWs grown in the direction [110] (a)–(g) and grown in the direction [111] (h)–(i) (a) $1\times1$, $Ge_{12}$, (b) $2\times2$, $Ge_{32}$, (c) $2\times3$, $Ge_{48}$, (d) $3\times3$, $Ge_{60}$, (e) $3\times4$, $Ge_{76}$, (f) $4\times4$, $Ge_{96}$, (g) $5\times5$, $Ge_{140}$, (h) $2\times2$, $Ge_{74}$, and (i) $2\times3$, $Ge_{138}$. The Fermi level is set to zero and is shown by the dotted line.

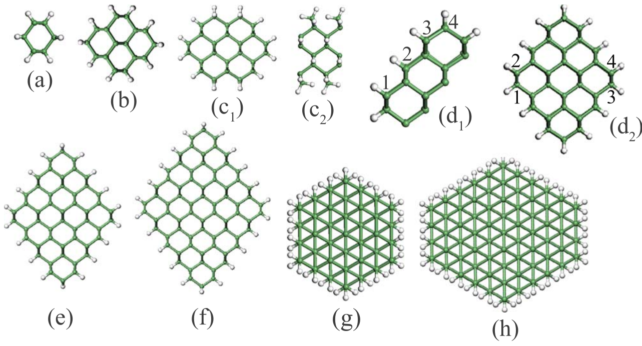


FIG. 3. (Color online) Cross-sectional views of the optimized hydrogen-passivated Ge NWs along the [110] [(a)–(f)] and [111] [(g)–(h)] directions. (a) $1\times1$, $Ge_{12}H_{16}$, (b) $2\times2$, $Ge_{32}H_{24}$, (c) $2\times3$, $Ge_{48}H_{32}$ top and side views, (d) $3\times3$, $Ge_{60}H_{28}$ top and substitution sites, (e) $4\times4$, $Ge_{28}Si_{68}H_{40}$, (f) $5\times5$, $Ge_{140}H_{48}$, (g) $2\times2$, $Ge_{74}H_{42}$, and (h) $2\times3$, $Ge_{138}H_{58}$. Green circles represent Ge atoms and white circles represent H atoms used for saturation of dangling bonds.

in which study Ge nanowires with diameters of 1.6 and 2.2 nm are metallic, a larger wire (diameter of 2.5 nm) being semiconducting with 0.17 eV. To the contrary, in a bare Si NW investigation[40] it is the smallest diameter wires that are semiconductor, similarly to the present case. Therefore, more analysis should certainly be carried on nanowires with different orientations, having different diameters and geometries to explain this fundamental difference.

The geometries of hydrogen passivated Ge NWs are shown in Fig. 3. The optimized structures are not subject to surface reconstruction as the surface dangling bonds are saturated. There is, however, an important surface relaxation effect, in particular onto the H-Ge-H bond angles that range between 103.6° and 107.5°. There is a small contraction in the Ge-Ge bond length (~1.0%) when going from the core to the surface. The average length of the Ge-H bond is 1.6 Å. For the [110]-$Ge_{48}H_{32}$ NW there is an interesting feature on the optimized structure, i.e., Ge atoms bonded with two hydrogen atoms deviate from the diamond [110] plane and produce a tilt of the Ge-H bonds with respect to the surface. This is an effect of the repulsion between H atoms born by neighboring Ge atoms since the tilting increases the H-H distance. This is not only reducing the symmetry of the wire but it is also strongly affecting the Ge-Ge-Ge bond angles in the first subsurface layer.

Figure 4 presents the energy band structures of hydrogen-passivated Ge NWs oriented along the [110] and [111] directions. For the present NWs, since the diameters are very small in comparison with the bulk Ge exciton Bohr radius (that is equal to 15 and 30 nm,[43] depending on the chosen band), the quantum confinement effect is expected to give the dominant contribution to the band-gap energies. As expected, the passivation of the dangling bonds with hydrogen removes the surface states observed in Fig. 2 outside of the band gap. With the increase in the wire diameter, from 0.6 to 2.9 nm for the [110] orientation, we observe an increase in the valence-band maximum (VBM) energy (2.3 eV) together with a decrease in the conduction-band minimum (CBM) energy (1.44 eV). The resulting reduction in the band-gap

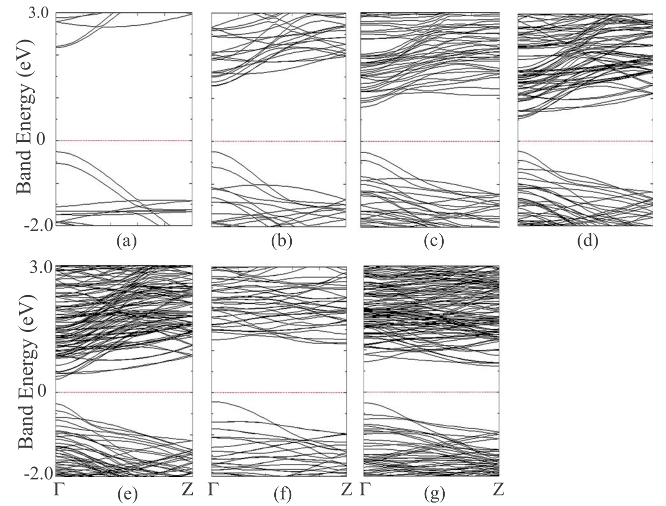


FIG. 4. (Color online) Energy band structures of hydrogenated-Ge NWs grown in the direction [110] (a)–(e) and grown in the direction [111] (f)–(g). The Fermi level is set to zero and is shown by the dotted line. (a) $Ge_{12}H_{16}$, (b) $Ge_{32}H_{24}$, (c) $Ge_{60}H_{28}$, (d) $Ge_{96}H_{40}$, (e) $Ge_{140}H_{48}$, (f) $Ge_{74}H_{42}$, and (g) $Ge_{138}H_{58}$.

energy is in coherent with the quantum confinement having a smaller effect for larger NW diameters (see Fig. 4). From the data in Table II, we can extrapolate from a linear fit of $E_g(\sqrt[3]{N_{Ge}})$ that the nanowire gap will reach the theoretical bulk value for a diameter of about 3.5 nm (see Fig. 5). This critical diameter value is close to that obtained for Ge nanocrystals by Hill *et al.*[44] It is also clear from the band-energy structures in Fig. 4 that the band gaps can be either direct or indirect according to the [110] or [111] orientation of the wire. The result is consistent with the values published in Refs. 14, 15, and 45.

The binding energies of H with respect to a free hydrogen atom are presented in Table II as computed by the following formula:

TABLE II. Binding energy ($E_b$ in eV/H atom) and band gaps ($E_g$ in eV) of hydrogen-passivated Ge NW with different orientations and diameters ($d$, in nm). Band gaps are denoted as follows: D for direct and I for indirect band gaps. While the direct gaps occur at the Γ point, indirect gaps take place between the VBM at Γ point and the CBM at (0,0,0.5) along the $z$ direction.

| Wire axis | $d$ (nm) | Number of Ge atoms | Number of H atoms | $E_b$ (eV) | $E_g$ (eV) | Type of band gap |
|---|---|---|---|---|---|---|
| [110] | 0.6 | 12 | 16 | −2.38 | 2.44 | D |
| | 1.2 | 32 | 24 | −2.53 | 1.54 | D |
| | 1.5 | 48 | 32 | −2.53 | 1.52 | D |
| | 1.9 | 60 | 28 | −2.61 | 1.05 | D |
| | 1.9 | 76 | 40 | −2.62 | 0.93 | D |
| | 2.4 | 96 | 40 | −2.66 | 0.77 | D |
| | 2.9 | 140 | 48 | −2.68 | 0.58 | D |
| [111] | 1.6 | 74 | 42 | −2.64 | 1.38 | I |
| | 2.4 | 138 | 58 | −2.63 | 0.87 | I |

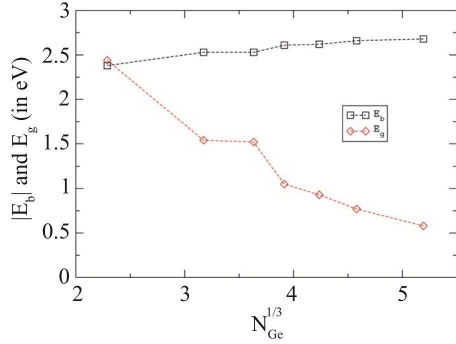


FIG. 5. (Color online) Absolute values of the binding energy ($E_b$) and band-gap energy ($E_g$) as a function of $\sqrt[3]{N_{\mathrm{Ge}}}$ for H-passivated Ge NWs grown in the [110] directions. The dashed lines are guide to the eyes to follow the trend.

$$E_b = (E[\mathrm{Ge}]_{\mathrm{NW+H}} - E[\mathrm{Ge}]_{\mathrm{NW}})/n_{\mathrm{H}} - E[\mathrm{H}]_{at}, \tag{2}$$

where $E[\mathrm{Ge}]_{\mathrm{NW}}$ and $E[\mathrm{Ge}]_{\mathrm{NW+H}}$ are the total energy of bare and hydrogen-passivated Ge NWs, respectively, and $n_{\mathrm{H}}$ is the total number of H atoms in the NW. The negative binding-energy points out the exothermic behavior of the binding of H atoms. As it can be seen in Table II, the absolute value of the binding energy increases gradually with the increase in the NW diameter.

Impurity atoms existing in NWs have a strong effect on the band structure and the band-gap energy. This effect can also be desirable to extend the range of the possible device applications. Although many studies have been published about doped Si NWs, especially the *n*- or *p*-type doping and the doping with transition metal atoms,[40,46–49] this is not the case for Ge NWs.[14,50] Whereas it was shown in the Ref. 14 that doping the core of Ge NWs with B (*p*-type) and P (*n*-type) atoms causes a VBM (CBM) increase (decrease) in energy, without any remarkable dispersion of the bands, Wang *et al.*[50] observed experimentally the band bending properties of *p*- and *n*-type doped oxidized Ge NWs. In the present study, we first considered the Si doping of Ge NW by substituting Si atoms on the hydrogenated surfaces. By increasing the number of Si dopants on the surface, we move from pure Ge to doped Ge NW and finally reach effectively a Ge/Si core-shell NW configuration. For the sake of comparison, we also considered the symmetrical Si/Ge core-shell wire in specific cases. The initial system is the unsubstituted [110]-$Ge_{60}H_{28}$ nanowire which is constructed from a $3\times3$ diamond supercell. As a first step, one Si atom dopant is added to the system by substituting one Ge atom located at any of four different doping sites [see Fig. 3($d_1$)]. The most favorable doping site is found to be the position 1. Then, the two atoms are placed at equivalent positions and again site 1 is the most stable surface site. These results can be intuitively understood if one notices that the Ge-Ge bonds around site 1 are on average shorter than around the other sites, so that the substitution by the smaller silicon atom induces less change in the network. For eight Si atoms doping, three different configurations have been considered and the most favorable doping sites are found to be the ones shown in Fig. 3($d_2$), the four other Si atoms being placed at equivalent positions.

TABLE III. Band-gap energies of Si-doped Ge, Ge/Ge-Si, and Ge/Si and Si/Ge core/shell NWs vs wire geometries.

| Type of NW | Shape of NW | System | $E_g$ (eV) |
|---|---|---|---|
| Si-doped Ge | $3\times3$ | $Ge_{59}Si_1H_{28}$ | 1.06 |
| Si-doped Ge | $3\times3$ | $Ge_{58}Si_2H_{28}$ | 1.07 |
| Si-doped Ge | $3\times3$ | $Ge_{52}Si_8H_{28}$ | 1.12 |
| Ge/Ge-Si core/shell | $3\times3$ | $Ge_{30}Si_{30}H_{28}$ | 1.20 |
| Ge/Si core/shell | $3\times3$ | $Ge_{12}Si_{48}H_{28}$ | 1.20 |
| Si/Ge core/shell | $3\times3$ | $Ge_{48}Si_{12}H_{28}$ | 1.18 |
| Ge/Si core/shell | $4\times4$ | $Ge_{36}Si_{60}H_{40}$ | 0.88 |
| Ge/Si core/shell | $4\times4$ | $Ge_{28}Si_{68}H_{40}$ | 0.83 |
| Ge/Si core/shell | $4\times4$ | $Ge_{16}Si_{80}H_{40}$ | 0.89 |
| Ge/Si core/shell | $4\times4$ | $Ge_4Si_{92}H_{40}$ | 0.92 |
| Si/Ge core/shell | $4\times4$ | $Ge_{68}Si_{28}H_{40}$ | 0.72 |
| Ge/Si core/shell | $5\times5$ | $Ge_{48}Si_{92}H_{48}$ | 0.68 |

Table III presents the geometries and band-gap energies of different NWs. The increase in the number of substitutional Si on the surface ends up in a complete Si shell formation. This goes with an increase in the band-gap energy. For $4\times4$-shaped NWs, the same trend in $E_g$ is seen but [110]-$Ge_{28}Si_{68}H_{40}$ slightly deviates from this rule. This is coherent with the fact that bulk Si has a larger gap than bulk Ge.

Moreover, Si/Ge core/shell NWs have smaller band gaps than Ge/Si core/shell ones having the same number of core and shell atoms. The quantum confinement effect is still observed for the core/shell NWs that we studied. For very close compositions (i.e., similar $N_{core}/(N_{core}+N_{shell})$ ratios, where $N_{core}$ and $N_{shell}$ are the number of core and shell atoms, respectively) as the diameter of the NW increases the band-gap energy decreases as expected.

Energy band-gap structures are shown in Fig. 6. Whereas $3\times3$ shaped NWs have flatlike conduction bands away from $\Gamma$, $4\times4$ NWs have more parabolic shapes. All of the NWs are found to have direct band gaps at the $\Gamma$ point. It can be noticed that as the width of Si-shell increases, the conduction-band minimum energy increases and valence-band maximum energy decreases at the Z point indicating the dominant contribution of the Si atoms to the upper valence and lower conduction states at this point. Migas and Borisenko[28] have found similar results for Ge/Si core/shell structures. They found that Ge/Si core/shell NWs without surface dimer reconstructions had direct band gaps and a behavior of the conduction band at Z point that is similar to the present study.

To understand the contributions of the atoms to the valence and conduction bands, the spatial localizations of the wave functions are plotted and presented in Fig. 7. Among the many NW configurations, we present three different diameters for the two orientations to demonstrate the diversity between the wave functions and extract some trends. Figures 6(a) and 6(e) show H-passivated Ge NWs oriented along the

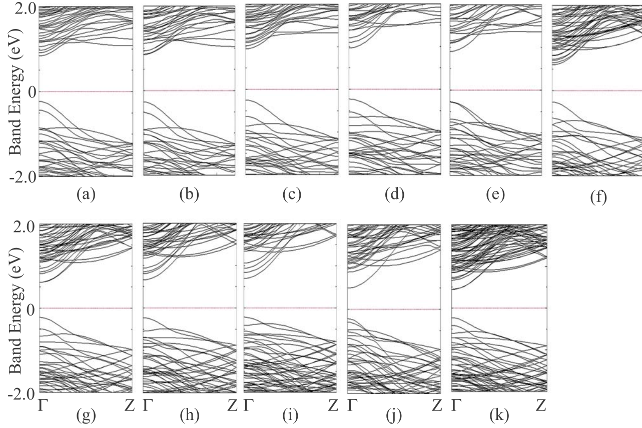


FIG. 6. (Color online) Energy band structures of Si-doped Ge NWs, (a) and (b), Ge/Ge-Si core/shell NWs, (c), Ge/Si core/shell NWs, (d), (f)–(i), (k), and Si/Ge core/shell NWs, (e) and (j) grown in the [110] direction. $3\times3$ structures are presented in (a)–(e), $4\times4$ are in (f)–(j) and $5\times5$ is in (k). The Fermi level set to zero and is shown by the dotted line. (a) $Ge_{58}Si_2H_{28}$, (b) $Ge_{52}Si_8H_{28}$, (c)$Ge_{30}Si_{30}H_{28}$, (d) $Ge_{12}Si_{48}H_{28}$, (e) $Ge_{48}Si_{12}H_{28}$, (f) $Ge_{36}Si_{60}H_{40}$, (g) $Ge_{28}Si_{68}H_{40}$, (h) $Ge_{16}Si_{80}H_{40}$, (i) $Ge_4Si_{92}H_{40}$, (j) $Ge_{68}Si_{28}H_{40}$, and (k) $Ge_{48}Si_{92}H_{48}$.

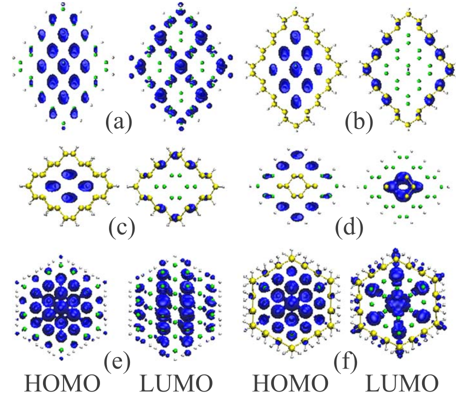


FIG. 7. (Color online) HOMO and LUMO charge densities for the H-passivated Ge NWs, Ge/Si, and Si/Ge core/shell NWs are shown. Green, yellow, and gray balls represent Ge, Si, and H atoms, respectively. (a) $Ge_{96}H_{40}$, (b) $Ge_{36}Si_{60}H_{40}$, (c) $Ge_{16}Si_{44}H_{28}$, and (d) $Ge_{44}Si_{16}H_{28}$ are grown along [110] direction, and (e) $Ge_{74}H_{42}$ and (f) $Ge_{38}Si_{36}H_{42}$ are grown along [111] direction.

[110] and [111] directions, respectively. While both NWs have HOMO distributions mainly located in the core and spreading through the shell, the LUMO of [110] NW is delocalized in the core and the shell and the [111]-LUMO is quite similar to its HOMO counterpart. These results are consistent with the study of Arantes and Fazzio.[15] The HOMO and LUMOs of the core/shell structures (b)–(d) are very different. The HOMOs are localized on Ge atoms (at the Γ point), but the LUMOs are preferentially localized on Si atoms independent of whether these are located in the core or in the shell. On the other hand, the [111] oriented core/shell NW (f) does not show this spatial carrier localization and HOMO-LUMO distributions are mainly localized in the core. In a very recent investigation, a similar carrier localization has been observed for asymmetric SiGe NWs oriented in the [110] direction, the valence-band maximum state was located on the Ge side of the wire and the conduction-band minimum was localized on the Si side.[51] The results from Fig. 7 make it clear that the eventual electron-hole separation in core/shell NWs is highly dependent on the orientation, which has a significant importance in the solar-energy conversion technology.

We further describe the electronic structure properties around the conduction-band minimum and valence-band maximum by determining the effective masses of both electrons and holes. The effective masses provide useful information for the potential use of these wires in optical devices such as quantum well infrared photodetectors and light emitting and laser diodes. The effective mass proves to be very sensitive to atomic substitution in the present case. The electron and hole effective masses can be simply calculated as the inverse of the curvature of the conduction-band minimum

$$m_e^* = \pm \hbar^2 \left( \frac{d^2E}{dk^2} \right)^{-1}, \tag{3}$$

where plus and minus signs are used for electron and hole effective mass calculations.

In the literature there are many studies of the effective masses of Si, Ge, and SiGe alloys.[52–54] Table IV presents the calculated electron and hole effective masses for Ge NWs,

TABLE IV. Electron ($m_e^*$) and hole ($m_h^*$) effective masses are presented. $N$ is the total number of atoms in NWs and $x$ is the fraction of core Ge(Si) atoms in the NWs [$x=N_{Ge(Si)}/(N_{Ge}+N_{Si})$]. The middle and right columns are for Ge/Si and Si/Ge core/shell NWs. The system size is represented by $\sqrt[3]{N_{Ge}}$ which is directly proportional to the NW diameter.

| Structure | $\sqrt[3]{N}$ | $m_e^*$ | $m_h^*$ | Structure | $x$ | $m_e^*$ | $m_h^*$ | Structure | $x$ | $m_e^*$ | $m_h^*$ |
|---|---|---|---|---|---|---|---|---|---|---|---|
| $Ge_{12}H_{16}$ | 3.04 | 0.333 | 0.304 | $Ge_{12}Si_{48}H_{28}$ | 0.20 | 0.346 | 0.423 | $Ge_{80}Si_{16}H_{40}$ | 0.17 | 0.343 | 0.191 |
| $Ge_{32}H_{24}$ | 3.83 | 0.323 | 0.265 | $Ge_{30}Si_{30}H_{28}$ | 0.50 | 0.346 | 0.311 | $Ge_{68}Si_{28}H_{40}$ | 0.29 | 0.348 | 0.204 |
| $Ge_{60}H_{28}$ | 4.45 | 0.312 | 0.259 | $Ge_{52}Si_8H_{28}$ | 0.87 | 0.345 | 0.256 | $Ge_{60}Si_{36}H_{40}$ | 0.38 | 0.342 | 0.212 |
| $Ge_{76}H_{40}$ | 4.88 | 0.241 | 0.187 | $Ge_{58}Si_2H_{28}$ | 0.97 | 0.315 | 0.253 | | | | |
| $Ge_{96}H_{40}$ | 5.14 | 0.230 | 0.181 | $Ge_4Si_{92}H_{40}$ | 0.04 | 0.353 | 0.408 | | | | |
| $Ge_{140}H_{48}$ | 5.73 | 0.168 | 0.148 | $Ge_{16}Si_{80}H_{40}$ | 0.17 | 0.349 | 0.341 | | | | |
| | | | | $Ge_{28}Si_{68}H_{40}$ | 0.29 | 0.375 | 0.315 | | | | |
| | | | | $Ge_{36}Si_{60}H_{40}$ | 0.37 | 0.337 | 0.258 | | | | |

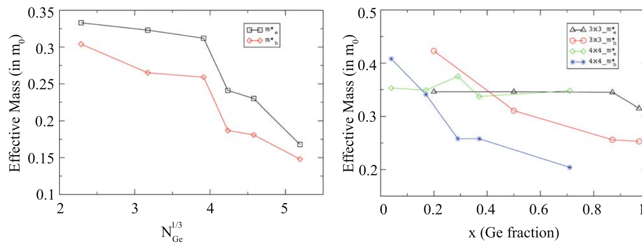

FIG. 8. (Color online) Effective mass versus $\sqrt[3]{N_{\mathrm{Ge}}}$ for H-passivated Ge NWs (left) and fraction of Ge atoms in H-passivated GeSi NWs (right).

Ge/Si, and Si/Ge core/shell NWs. For very small diameters both effective masses are very large but as the diameter increases they decrease. For Ge NW, the longitudinal electron effective mass seems to converge toward its experimental Ge bulk value $(0.082m_0)$ and the heavy hole effective mass remains smaller than its bulk value $(0.34m_0)$.[55] This finding is consistent with the study of Bescond *et al.*[56] in which the effective masses of [100]-Ge NWs have been calculated using a tight-binding model. The effective masses of the core/shell NWs can be compared to the Ge(Si) core composition in the NWs. The electron effective masses do not vary significantly with the formation of a Si(Ge) shell (see Fig. 8). This is not the case for the hole effective masses which decrease (increase) with the ratio of the core/shell thicknesses. This behavior is similar to that of hole effective masses in strained $Si_{1-x}Ge_x/Si$ quantum layers.[53]

## IV. CONCLUSION

Using density-functional theory, we have studied the structural and electronic properties of bare Ge NWs, H-passivated Ge NWs, Si-doped Ge NWs and Ge/Si core/shell NWs aligned in the [110] and [111] directions for diameters up to 2.9 nm. It is found that the orientation and the diameter have significant effects on the electronic properties of NWs. The bare Ge NWs having very small diameters are found to be semiconducting and larger ones are metallic. However, it should be noted again that because GGA yields a zero Ge bulk band gap, small diameter Ge NWs could potentially be semiconductor as well. This issue should motivate further investigation with more accurate methods that include many-body corrections, such as the GW method. However, our calculations indicate clear trends among the various types of wires, with respect to the composition, orientation and diameter. The dangling-bond passivation with H atoms caused the NWs grown in [110] direction to have direct band gaps and the NWs with [111] orientation to have indirect band gaps. Moreover, H-passivated Ge NWs exhibit a strong quantum confinement effect which remains significant upon the formation of a Si shell. However, the details of the electronic structure are strongly affected by the progressive substitution with silicon atoms, especially regarding the holes effective masses. This work also emphasizes the importance of the orientation for the optical properties of NWs since the wave-function spatial localizations of the uppermost valence and lowest conduction bands are extremely different according to the wire axis orientation. This spatial confinement of electrons and holes to the shell and core of NWs could allow these materials to be suitable for photovoltaic or photoconduction applications. Therefore, the [110] oriented Ge/Si core/shell wires appear to be the most promising ones due to their spatial separation of carriers in terms of their potential applications in optical and electronic areas.

## ACKNOWLEDGMENTS

This work is supported by the Belgian FNRS through the FRFC Convention No. 2.4505.09.

*rpekoz@ulg.ac.be


[1] X. Duan, Y. Huang, Y. Cui, J. Wang, and C. M. Lieber, Nature (London) **409**, 66 (2001).
[2] T. Someya, R. Werner, A. Forchel, M. Catalano, R. Cingolani, and T. Arakawa, Science **285**, 1905 (1999).
[3] Y. Huang, X. Duan, Y. Cui, L. J. Lauhon, K.-H. Kim, and C. M. Lieber, Science **294**, 1313 (2001).
[4] Y. Cui, Z. Zhong, D. Wang, W. U. Wang, and C. M. Lieber, Nano Lett. **3**, 149 (2003).
[5] J. Xiang, W. Lu, Y. J. Hu, Y. Wu, H. Yan, and C. M. Lieber, Nature (London) **441**, 489 (2006).
[6] A. Hagfeldt and M. Grätzel, Chem. Rev. (Washington, D.C.) **95**, 49 (1995).
[7] B. Tian, X. Zheng, T. J. Kempa, Y. Fang, N. Yu, G. Yu, J. Huang, and C. M. Lieber, Nature Lett. **449**, 885 (2007).
[8] M. R. Lee, R. D. Eckert, K. Forberich, G. Dennler, C. J. Brabec, and R. A. Gaudiana, Science **324**, 232 (2009).
[9] K. Hiruma, M. Yazawa, T. Katsuyama, K. Ogawa, K. Haraguchi, M. Koguchi, and H. Kakibayashi, J. Appl. Phys. **77**, 447 (1995).
[10] W. Q. Han, S. S. Fan, Q. Q. Li, and Y. D. Hu, Science **277**, 1287 (1997).
[11] D. D. D. Ma, C. S. Lee, F. C. K. Au, S. Y. Tong, and S. T. Lee, Science **299**, 1874 (2003).
[12] X. Zhao, C. M. Wei, L. Yang, and M. Y. Chou, Phys. Rev. Lett. **92**, 236805 (2004).
[13] H. Adhikari, A. F. Marshall, C. E. D. Chidsey, and P. C. McIntyre, Nano Lett. **6**, 318 (2006).
[14] D. Medaboina, V. Gade, S. K. R. Patil, and S. V. Khare, Phys. Rev. B **76**, 205327 (2007).
[15] J. T. Arantes and A. Fazzio, Nanotechnology **18**, 295706 (2007).
[16] C. Harris and E. P. O'Reilly, Physica E (Amsterdam) **32**, 341 (2006).
[17] Y. Cui, L. J. Lauhon, M. S. Gudiksen, J. Wang, and C. M. Lieber, Appl. Phys. Lett. **78**, 2214 (2001).
[18] J. D. Holmes, K. P. Johnston, R. C. Doty, and B. A. Korgel, Science **287**, 1471 (2000).
[19] J. Noborisaka, J. Motohisa, S. Hara, and T. Fukui, Appl. Phys. Lett. **87**, 093109 (2005).

[20] L. V. Titova, T. B. Hoang, H. E. Jackson, L. M. Smith, J. M. Yarrison-Rice, and Y. Kim, Appl. Phys. Lett. **89**, 173126 (2006).

[21] M. Law, L. E. Greene, A. Radenovic, T. Kuykendall, J. Liphardt, and P. D. Yang, J. Phys. Chem. B **110**, 22652 (2006).

[22] J. Li, D. Zhao, X. Meng, Z. Zhang, J. Zhang, D. Shen, Y. Lu, and X. Fan, J. Phys. Chem. B **110**, 14685 (2006).

[23] V. Radmilovic, M. Law, P. Yang, A. Radenovic, and C. E. Nelson, Microsc. Microanal. **12**, 474 (2006).

[24] H.-M. Lin, Y.-L. Chen, J. Yang, Y.-C. Liu, K.-M. Yin, J.-J. Kai, F.-R. Chen, L.-C. Chen, Y.-F. Chen, and C.-C. Chen, Nano Lett. **3**, 537 (2003).

[25] Y. Zhang, L.-W. Wang, and A. Mascarenhas, Nano Lett. **7**, 1264 (2007).

[26] L. J. Lauhon, M. S. Gudiksen, D. Wang, and C. M. Lieber, Nature (London) **420**, 57 (2002).

[27] R. N. Musin and X.-Q. Wang, Phys. Rev. B **74**, 165308 (2006).

[28] D. B. Migas and V. E. Borisenko, Phys. Rev. B **76**, 035440 (2007).

[29] Different orientations in NWs are extensively studied and for both Si and Ge wires aligned in the [110] direction are found to have the smallest band gap and [100] have the largest (Ref. 16).

[30] In the literature there are many definitions for defining the diameter of NWs. In this study, the diameters are given in terms of the largest distance between two hydrogen atoms.

[31] W. Kohn and L. J. Sham, Phys. Rev. **140**, A1133 (1965).

[32] P. E. Blochl, Phys. Rev. B **50**, 17953 (1994).

[33] J. P. Perdew and Y. Wang, Phys. Rev. B **45**, 13244 (1992).

[34] J. P. Perdew, J. A. Chevary, S. H. Vosko, K. A. Jackson, M. R. Pederson, D. J. Singh, and C. Fiolhais, Phys. Rev. B **46**, 6671 (1992).

[35] Numerical computations have been carried out by using VASP software: G. Kresse and J. Hafner, Phys. Rev. B **47**, 558 (1993); G. Kresse and J. Furthmüller, *ibid.* **54**, 11169 (1996).

[36] C. Filippi, D. J. Singh, and C. J. Umrigar, Phys. Rev. B **50**, 14947 (1994).

[37] S. Q. Wang and H. Q. Ye, J. Phys.: Condens. Matter **15**, L197 (2003).

[38] E. R. Batista, J. Heyd, R. G. Hennig, B. P. Uberuaga, R. L. Martin, G. E. Scuseria, C. J. Umrigar, and J. W. Wilkins, Phys. Rev. B **74**, 121102(R) (2006).

[39] H. J. Monkhorst and J. D. Pack, Phys. Rev. B **13**, 5188 (1976).

[40] E. Durgun, N. Akman, and S. Ciraci, Phys. Rev. B **78**, 195116 (2008).

[41] In the literature these types of geometries are studied for Ge, Si, and Ge/Si NWs (Refs. 15 and 51). In the present calculations the effect of unit cell is also studied for $3\times3$ $Ge_{60}$ NW grown in the [110] direction. In the double cell calculations, after the optimization, the same atomic configuration and a very slight change in the cohesive energy per Ge atom (0.004 eV) was found. Therefore, all other calculations were performed with single unit cells.

[42] C. Kittel, *Introduction to Solid State Physics*, 7th ed. (John Wiley & Sons, Singapore, 1996).

[43] M. L. Cohen and J. R. Chelikowsky, *Electronic Structure and Optical Properties of Semiconductors* (Springer, Berlin, 1988).

[44] N. A. Hill, S. Pokrant, and A. J. Hill, J. Phys. Chem. B **103**, 3156 (1999).

[45] M. Bruno, M. Palummo, A. Marini, R. Del Sole, V. Olevano, A. N. Kholod, and S. Ossicini, Phys. Rev. B **72**, 153310 (2005).

[46] M.-V. Fernandez-Serra, Ch. Adessi, and X. Blase, Nano Lett. **6**, 2674 (2006).

[47] F. Iori and S. Ossicini, Physica E (Amsterdam) **41**, 939 (2009).

[48] A. K. Singh, V. Kumar, R. Note, and Y. Kawazoe, Nano Lett. **6**, 920 (2006).

[49] H. Sellier, G. P. Lansbergen, J. Caro, S. Rogge, N. Collaert, I. Ferain, M. Jurczak, and S. Biesemans, Phys. Rev. Lett. **97**, 206805 (2006).

[50] D. Wang, Y. L. Chang, Q. Wang, J. Cao, B. Farmer, R. G. Gordon, and H. Dai, J. Am. Chem. Soc. **126**, 11602 (2004).

[51] M. Amato, M. Palummo, and S. Ossicini, Phys. Rev. B **79**, 201302(R) (2009).

[52] W. G. Spitzer and H. Y. Fan, Phys. Rev. **106**, 882 (1957).

[53] J. P. Cheng, V. P. Kesan, D. A. Grutzmacher, and T. O. Sedgwick, Appl. Phys. Lett. **64**, 1681 (1994).

[54] T. B. Boykin, G. Klimeck, and F. Oyafuso, Phys. Rev. B **69**, 115201 (2004).

[55] G. Dresselhaus, A. F. Kip, and C. Kittel, Phys. Rev. **98**, 368 (1955).

[56] M. Bescond, N. Cavassilas, K. Nehari, and M. Lannoo, J. Comput. Electron. **6**, 341 (2007).